

# Analytical insights into the transient climate response

Boriana Chtirkova<sup>a, b</sup>

<sup>a</sup> *Department of Geosciences, Princeton University, Princeton, New Jersey*

<sup>b</sup> *Program in Atmospheric and Oceanic Sciences, Princeton University, Princeton, New Jersey*

arXiv:2603.01674v1 [physics.ao-ph] 2 Mar 2026

*Corresponding author:* Boriana Chtirkova, chtirkova@princeton.edu

ABSTRACT: The temperature in the transient climate response is lower than the equilibrium temperature for the same amount of forcing. The degree of disequilibrium is not constant in time and depends on various climate parameters. We derive intuition for this by solving the heat equation with a surface temperature feedback for linearly increasing forcing. The surface temperature initially evolves at a slower rate than the corresponding steady state (SS) temperature and it accelerates until quasi-steady state (QSS), when the SS and QSS temperatures evolve in parallel with a constant offset. The offset depends on the rate of forcing and total heat capacity of the system divided by the square of the climate feedback. The timescale over which the climate system approaches QSS depends also on the effective ocean mixing and is order of thousands of years. Over societally relevant timescales ( $\sim 100$  years), the top-of-atmosphere energy imbalance increases, and the actual temperature moves farther from the steady-state temperature expected for the same forcing.

**SIGNIFICANCE STATEMENT:** Understanding why the transient climate response differs from equilibrium climate sensitivity is essential for interpreting near-term climate change. By solving a diffusive ocean model with a surface temperature feedback under linearly increasing forcing, we show that the climate system moves progressively further from equilibrium over societally relevant timescales, accompanied by an evolving top of atmosphere energy imbalance. We provide a simple, physically transparent framework on the roles of the surface temperature feedback and effective ocean mixing in shaping the temporal evolutions of temperature and the top of the atmosphere imbalance.

## **1. Introduction**

The temperature response to a transient increase in the forcing is always lower than the temperature, which the system will approach if the forcing is fixed after a certain point in time. To address the question whether, at the time of their analysis, the observed warming is consistent with the forcing, Wigley and Schlesinger (1985) discuss an analytical solution of the thermal diffusion equation that describes the evolution of the surface temperature of a system with large thermal inertia. They show that at any given point the forced climate system can be quite far from equilibrium, and they derive the degree of disequilibrium to depend on the climate feedback and the effective ocean diffusivity, representing the vertical ocean mixing. A similar problem setup has been investigated by Lebedeff (1988); Watts et al. (1994); Morantine and Watts (1994) for either a mixed layer or a full ocean. The response timescale is shown to depend on the assumptions of the domain depth and the climate feedback parameter, yielding a timescale on the order of a few hundred years.

We revisit the problem of interpretation of the temperature state of the climate system after an order of 100 years of forcing using a diffusion model, but with energy conserving boundary conditions and a finite depth of the diffusive column emulating the ocean heat reservoir. In this setup, the heat equation becomes a continuous form of the frequently used two-box model (Gregory 2000; Held et al. 2010). We provide a compact analytical expression for the surface temperature and top of atmosphere imbalance response to linearly increasing forcing. The timescale we estimate for the system to approach quasi-steady state depends on the domain depth and heat exchange coefficient but not on the climate feedback parameter and is on the order of a thousand years.

At present, the degree of disequilibrium is mostly inferred from atmosphere-ocean general circulation model (AOGCM) simulations. The adopted procedure is to estimate the temperature which the system approaches for a given amount of constant forcing  $T_{\text{ECS}}$  (e.g. from the abrupt-4xCO<sub>2</sub> experiment) and the temperature at a fixed point of a run with monotonically increasing forcing  $T_{\text{TCR}}$  (e.g. from the 1pctCO<sub>2</sub> experiment (Eyring et al. 2016)). These two temperatures are usually normalized to a doubling of the forcing ( $F_{2x}$ ) and are termed equilibrium climate sensitivity (ECS) and transient climate response (TCR). The definition of  $T_{\text{TCR}}$  as the temperature around the year of doubling of CO<sub>2</sub> emissions for a scenario with a growth rate of 1% per year<sup>1</sup> is a practical way to assess model results. However,  $T_{\text{TCR}}$  is a function of the forcing growth rate and may not scale linearly with the forcing, which is one of the concerns this paper investigates. Within coupled climate models, the ranges for ECS are between 1.8 – 5.6 K and for TCR between 1.3 – 3.0 K (IPCC 2023; Flynn and Mauritsen 2020; Nijssen et al. 2020; Meehl et al. 2020).

$T_{\text{TCR}}$ , unlike  $T_{\text{ECS}}$ , is not only a function of the climate feedback parameter, but is also influenced by ocean heat uptake (Hoffert et al. 1980; Wigley and Schlesinger 1985; Raper et al. 2002; Gregory and Forster 2008; Rose and Rayborn 2016), or more precisely, by how efficiently the ocean takes up heat over the time period used to evaluate the  $T_{\text{TCR}}$ . The ocean heat uptake can affect the transient climate response by changing the effective heat capacity of the system (Gregory and Forster 2008; Gregory et al. 2023) and by modulating the response of the atmosphere (Held et al. 2010; Winton et al. 2010; Rose and Rayborn 2016). Kostov et al. (2014) relate the Atlantic Meridional Overturning Circulation (AMOC) with the efficiency of ocean heat uptake and show that climate models with a stronger AMOC have a larger effective heat capacity and therefore lower  $T_{\text{TCR}}$ . Kuhlbrodt and Gregory (2012) highlight the importance of the eddy-induced thickness diffusivity parameter in climate models, which is particularly effective in the Southern Ocean. The Southern Ocean is estimated to be the ocean region with the largest increase in heat content (Frölicher et al. 2015). The efficiency with which the ocean propagates heat in depth is also related to the depth of the pycnocline (Newsom et al. 2023) and salinity distributions (Liu et al. 2023).

Simulations from coupled general circulation models with linearly increasing forcing indicate a linear evolution of the surface temperature in a period of 100-150 years after the onset of the forcing (e.g. Gregory (2000); Gregory and Forster (2008)). By rearranging the linear climate feedback

---

<sup>1</sup>Concentrations grow exponentially with a rate of 1 % per year:  $C(t) = C_0 1.01^t$ , the time  $t'$  at which  $C(t') = 2C_0$  is  $2 = 1.01^{t'}$ ,  $t' = \log_{1.01}(2) = \frac{\ln(2)}{\ln(1.01)} \approx 70$ .

equation:  $F(t) - \lambda\Delta T(t) = N(t)$ , where  $\Delta T(t)$  is the departure from the unperturbed temperature,  $\lambda$  is the climate feedback parameter,  $F$  is the additional forcing and  $N$  is the system imbalance, one obtains:

$$\Delta T(t) = \frac{F(t)}{\lambda + \frac{N(t)}{T(t)}} = \frac{F(t)}{\lambda + \kappa(t)}, \quad (1)$$

in which  $\kappa(t) = \frac{N(t)}{T(t)}$  is the definition of ocean heat uptake efficiency (Gregory 2000; Gregory and Forster 2008; Gregory et al. 2015, 2023). Since both the temperature and imbalance vary in time,  $\kappa$  will depend on the period over which it is evaluated and will vary from  $\kappa \rightarrow \infty$  in the beginning of the simulation to  $\kappa \rightarrow 0$  after sufficiently long (Gregory et al. 2023). For inter-model comparisons, it has become standard to evaluate  $\kappa$  from  $T_{\text{TCR}}$  around the year of doubling of the forcing and  $\kappa$  is often interpreted as an AOGCM-specific coefficient of thermal coupling coefficient between the upper and deep ocean.

A conceptual framework for investigating the climate response is a two-box diffusive model (Gregory 2000; Held et al. 2010; Winton et al. 2010), which is formulated as a system of two coupled ordinary differential equations:

$$\begin{cases} C_1 \frac{dT_1}{dt} = F - \lambda T_1 - \epsilon \gamma (T_1 - T_2) \\ C_2 \frac{dT_2}{dt} = \gamma (T_1 - T_2) \end{cases} \quad (2)$$

The forcing  $F$  at the top of the atmosphere acts on a layer with a heat capacity  $C_1$  and temperature  $T_1(t)$ , which transports heat to a lower layer with a heat capacity  $C_2$  and temperature  $T_2(t)$ . The upper layer may represent the well-mixed upper ocean, and the lower layer – the deep ocean, such that the system is commonly evaluated for  $C_1 \ll C_2$ . The heat flux between the two layers is proportional to their difference by a heat exchange coefficient  $\gamma$ . The system loses heat to space through a climate feedback parameter  $\lambda$  acting through the upper layer temperature. The full version of this model includes an efficacy factor  $\epsilon$  (Held et al. 2010; Winton et al. 2010), which modulates the heat loss to space. For the purpose of this paper we consider no such modulation, i.e.  $\epsilon = 1$ .

The 2-layer model (equation 2) recovers a linear relationship between the forcing and surface temperature in the limit  $C_1 \rightarrow 0$  and  $T_2 \rightarrow 0$  (or  $C_2 \rightarrow \infty$ ):

$$\lim_{C_1 \rightarrow 0, T_2 \rightarrow 0} T_1 = \frac{F(t)}{\lambda + \gamma}, \quad (3)$$

but by doing this one loses all time information and there are no estimates for the validity range of this approximation (Jeevanjee et al. 2025).

Within the 2-box model  $\gamma$  is a constant parameter, which unlike  $\kappa(t)$  does not vary in time; hence it is unclear what the physical interpretation of the two quantities should be. There is no standard procedure for diagnosing  $\gamma$  from climate models. One way would be to suppose the limit from equation 3 is valid in the year of forcing doubling and compute  $\gamma$  from  $T_{\text{TCR}} = T_1$ . A second approach is numerically fitting the coefficients of the two-layer model to AOGCM output, in which  $C_1$  is often treated as a free parameter, different from zero (e.g. Geoffroy et al. (2013b)). This raises questions about how estimates of  $\gamma$  obtained through different methods, i.e. supposing different heat capacities, should be interpreted.

We aim to provide a simple and physically transparent framework for an interpretation of the transient climate response under linearly increasing forcing. We ask why the evolution of surface temperature in a 150-year 1pctCO2 simulation appears linear, but its tendency is different from the steady-state temperature tendency ( $\frac{dF}{\lambda dt}$ ) and we bring together the dependence of the surface temperature evolution on the rate of forcing ( $\frac{dF}{dt} = a$ ) and the response time scale of the system. To do this, we investigate the analytical solution of the heat equation with energy conserving boundary conditions (section 2). We choose to analyze a continuous partial differential equation as opposed to the system of coupled ordinary differential equations (equation 2) because the former is a more general case and does not include  $C_1$  and  $C_2$  as free parameters, but we show that the two models are analogous (Appendix B). In section 3, we develop a physical intuition for the TCR problem through the concept of time-dependent apparent heat capacity. In section 4, we provide a method to estimate  $\gamma$  from AOGCMs by accounting for the response time scale of the system and making an assumption for the total heat capacity. Throughout the paper, we focus on both the surface temperature and the top of atmosphere imbalance.

## 2. Setup and solutions of the heat equation

We set up the classical heat (diffusion) equation in which temperature is a function of time and depth  $T = T(t, z)$ :

$$c \frac{\partial T}{\partial t} = K \frac{\partial^2 T}{\partial z^2} \quad (4)$$

For seawater, the volumetric heat capacity is  $c \approx 4 \times 10^6 \text{ Jm}^{-3}\text{K}^{-1}$  and the molecular diffusivity is  $K \approx 0.6 \text{ WK}^{-1}\text{m}^{-1}$  (Alexandrov et al. 2017). The molecular diffusivity is negligible compared to the effects of advection, convection, and mixing arising from wind stress, eddies, tides and bottom boundary layers. This turbulent mixing can be expressed as effective ocean diffusivity  $\kappa$  [ $\text{m}^2\text{s}^{-1}$ ] (Redi 1982; Gent and McWilliams 1990; Gnanadesikan 1999), applied either directly to the temperature field or indirectly through its effects on the velocity field. Estimates of global ocean diffusivity are usually built on theories which balance buoyancy with diffusivity. They suggest a vertical structure of  $\kappa$  being  $\sim 10^{-5} \text{ m}^2\text{s}^{-1}$  at mid-depths and  $\sim 10^{-4} \text{ m}^2\text{s}^{-1}$  in the abyss (Munk 1966; Munk and Wunsch 1998; Nikurashin and Vallis 2011; Rogers et al. 2023). A representative value of  $\kappa$  for the upper ocean is  $2.5 \times 10^{-5} \text{ m}^2\text{s}^{-1}$  and below 2500 meters it becomes larger than  $2 \times 10^{-4} \text{ m}^2\text{s}^{-1}$  due to the influence of orography. Relating these estimates of diffusivity directly to temperature (i.e.  $\kappa = \frac{K}{c}$ ) yields heat conductivity  $K \approx 100 - 800 \text{ WK}^{-1} \text{ m}^{-1}$ . The special case  $K(z) = K$  allows one to find an analytical solution that reveals the scalings needed to guide interpretation of climate model simulations where, as in the real ocean,  $K$  may be a function of depth, geographical location and time.

For an energy conserving system, the boundary conditions need to be formulated in terms of the fluxes at the top and bottom. The upper boundary is formulated using the forcing and a linear feedback so it contains both the function and its derivative in  $z$  (Robin boundary condition). The lower boundary condition says there is no flux out of the lower boundary (Neumann boundary condition).

$$\begin{aligned} z = 0: \quad \mathcal{F}(t, z = 0) &= -K \left. \frac{\partial T}{\partial z} \right|_{z=0} = F(t) - \lambda T(t, z = 0) = N(t), \lambda > 0 \\ z = L: \quad \mathcal{F}(t, z = L) &= -K \left. \frac{\partial T}{\partial z} \right|_{z=L} = 0 \end{aligned} \quad (5)$$

In this formulation, the upper boundary condition sets the heat tendency of the entire system. In climate science, it is referred to as the net top of the atmosphere (TOA) radiative flux, and for  $N \neq 0$  it is the TOA energy imbalance<sup>2</sup>. The values of the climate feedback parameter estimated from climate models are in the range  $0.6 - 1.5 \text{ Wm}^{-2}\text{K}^{-1}$  (IPCC 2023; Flynn and Mauritsen 2020; Nijssen et al. 2020). An appropriate value for the domain depth would be the effective ocean depth<sup>3</sup>  $L \approx 2600 \text{ m}$ . We adopt the convention of the flux being positive downward and  $z$  to increase in depth ( $z > 0$ ), hence the minus signs in the boundary conditions (equation 5).

### a. Steady-state solution

We first consider the case with constant forcing  $F(t > 0) = \text{const}$ . After sufficiently long the system will approach a steady state (SS), defined by  $\frac{\partial T(z)}{\partial t} = 0$ , in which the fluxes are in equilibrium and the temperature is constant in depth:

$$T_{\text{SS}}(z) = \frac{F}{\lambda} \quad (6)$$

For  $F = F_{2x}$ ,  $T_{\text{SS}}$  corresponds to the equilibrium climate sensitivity  $T_{\text{ECS}}$  commonly used in climate science.

### b. Quasi-steady state solution

For a linearly increasing forcing  $F = at$ ,  $\frac{dF}{dt} = a$ , the system has an analytical solution in which the terms containing  $t$  and  $z$  are separated:

$$T_{\text{QSS}}(t, z) = \frac{-2acKL + 2a\lambda Kt - 2a\lambda cLz + a\lambda cz^2}{2\lambda^2 K} = \frac{a}{\lambda}t + f(z) \quad (7)$$

with  $f(z) = \frac{-2acKL - 2a\lambda cLz + a\lambda cz^2}{2\lambda^2 K}$ . This solution describes a quasi-steady state (QSS), in which the temperature tendency across the whole domain is constant  $\frac{\partial T(z)}{\partial t} = \text{const} = \frac{a}{\lambda}$ , and the corresponding function of depth  $T(z) = f(z)$  is quadratic.

We can express the surface temperature and its offset from  $T_{\text{SS}}$  for each amount of forcing  $T_{\text{SS}}(t) = \frac{a}{\lambda}t$  as:

---

<sup>2</sup>The correct expression is for the temperature difference  $\Delta T_s$  relative to the pre-industrial global mean surface temperature. For simplicity, we set the initial temperature to 0 and omit the  $\Delta$  throughout the paper.

<sup>3</sup>From the mean depth of the ocean 3682 m times its surface area fraction 71%.

$$T_{\text{QSS}}(t, z = 0) = \frac{a}{\lambda}t - \frac{acL}{\lambda^2} = T_{\text{SS}}(t) - \frac{acL}{\lambda^2} \quad (8)$$

We note that  $T_{\text{QSS}}(t)$  is independent of heat conductivity  $K$ , but the time scale to reach the quasi-steady state is a function of  $K$  (see next section). This is different from solutions to the diffusion equation with a lower boundary condition  $T(t, z \rightarrow \infty) = 0$  as in Wigley and Schlesinger (1985), where such a QSS is never reached or  $T(t, z \rightarrow L) = 0$  as in Lebedeff (1988); Morantine and Watts (1994), in which the QSS surface temperature depends in addition to the heat conductivity coefficient  $K$  and the vertical structure function  $T(z)$  includes  $z^3$  terms in addition to the  $z^2$  terms. The same surface temperature QSS without  $K$  is derived as an asymptote for the diffusion equation solution by Watts et al. (1994). In the next section, we suggest a time scale to approach this QSS that is different from the one in Watts et al. (1994).

Figure 1 a,c presents  $T_{\text{SS}}$  and its parallel  $T_{\text{QSS}}$  at the surface (i.e.  $z = 0$ ) as black and gray dashed lines and Figure 1 c – the quadratic temperature profile in depth  $f(z)$  as red dashed line.

Since the temperature tendency is constant, the corresponding imbalance is also constant in time:

$$N_{\text{QSS}} = -K \left. \frac{\partial T}{\partial z} \right|_{z=0} = -K \left. \frac{-2a\lambda cL + 2a\lambda cz}{2\lambda^2 K} \right|_{z=0} = \frac{acL}{\lambda} \quad (9)$$

$N_{\text{QSS}}$  is time independent and depends on the system heat capacity and the rate of forcing. For an equivalent ocean depth  $L = 2600$  m and approximately the current rate of greenhouse gas forcing  $a = 0.04 \text{ Wm}^{-2}\text{yr}^{-1}$  (Smith et al. 2021), the TOA imbalance at QSS is  $N_{\text{QSS}} \approx \frac{13}{\lambda} \text{ Wm}^{-2}$ , which for any likely value of  $\lambda$  is higher than the currently observed  $1.0 \pm 0.2 \text{ Wm}^{-2}$  (Loeb et al. 2021, 2024), indicating that even after order 100 years of approximately linearly increasing forcing, Earth has not approached the QSS. In the following, we show that this result is consistent with the analytical solution for the timescale to reach QSS in the diffusion model (equations 4, 5).

### c. Approach to the QSS solution

If we add a zero initial condition to the system  $T(t = 0, z) = 0$ , the full solution is an infinite sum of time-decaying exponential modes:

$$T(t, z) = \frac{a}{\lambda}t - \sum_{i=1}^{\infty} f_i(z) e^{-t/\tau_i} \quad (10)$$

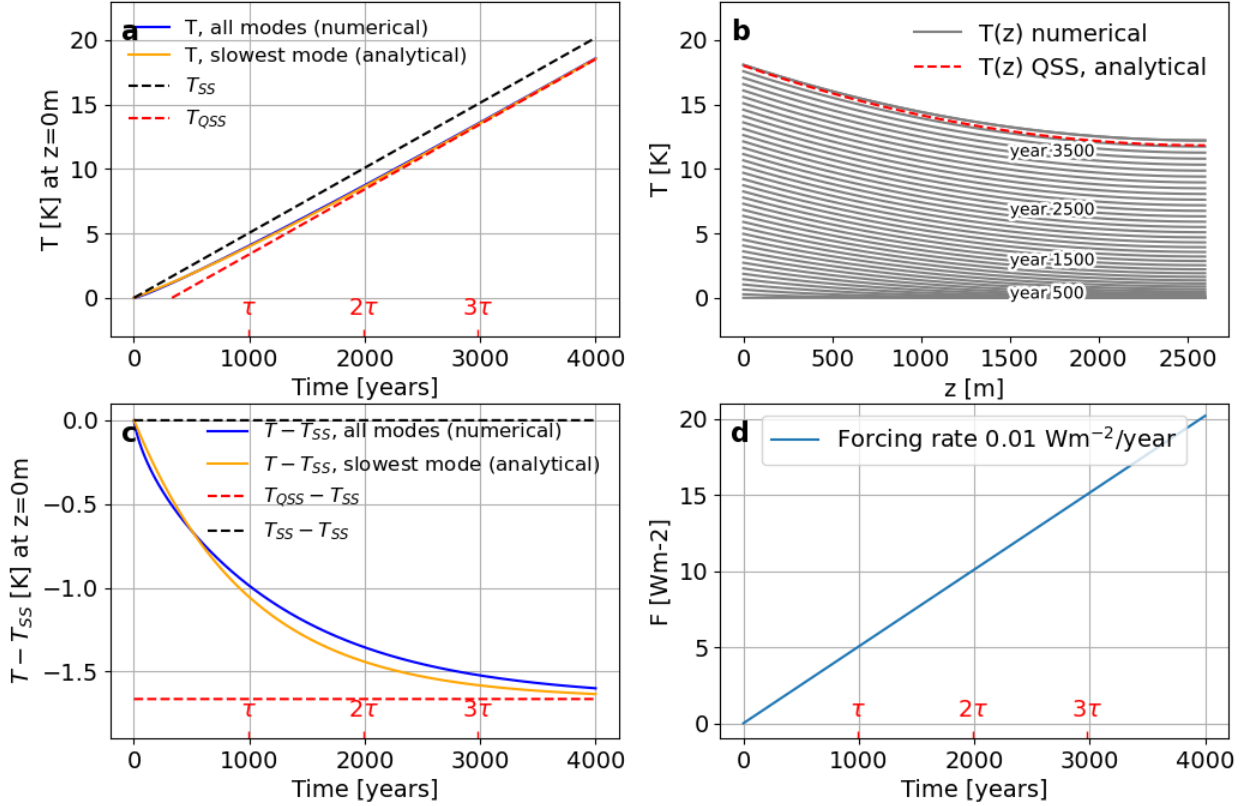


FIG. 1. Analytical (slowest decaying mode only) and numerical (all decaying modes) solutions to the heat equation with parameters  $F_{2\times} = 3.5 \text{ Wm}^{-2}$ ,  $\lambda = 1 \text{ Wm}^{-2}\text{K}^{-1}$ ,  $K = 350 \text{ Wm}^{-1}\text{K}^{-1}$ ,  $L = 2600 \text{ m}$  and a forcing increase of 1 permille/year. Evolution of surface temperature anomaly (a), corresponding temperature profiles in depth (b) - individual gray lines are 100 years apart, evolution of surface temperature anomaly relative to the steady state (SS) temperature (c), evolution of the forcing (d).

In Appendix A we show that in the limit  $\lambda L \gg K$ , one can approximate the timescale of the slowest decaying mode  $\tau_{sl}$  as

$$\tau_{sl} \approx \frac{c}{K} \frac{4L^2}{\pi^2} \quad (11)$$

Analysis of the orders of magnitude of the terms ( $L \sim 2 \times 10^3 \text{ [m]}$ ,  $\lambda \sim 1 \text{ [Wm}^{-2}\text{K}^{-1}]$ ,  $K \sim 10^2 - 10^3 \text{ [WK}^{-1}\text{m}^{-1}]$ ) yields  $\lambda L > K$ ; thus the approximation may not be expected to be highly accurate. Comparison with the numerical solution, which contains all modes (orange versus blue lines in Figures 1 - 2), shows that the approximation describes the surface temperature and system imbalance evolution reasonably well and is suitable to provide physical intuition. Using solely one

timescale to approximate the system response will reduce the curvature of the temporal evolution of the surface layers close to the onset of the forcing.

The timescale  $\tau_{sl}$  to approach the QSS with the quadratic form of the vertical structure function  $T(z)$  is a property of the system (i.e. a function of  $c, K, L$ ), and is independent of the forcing rate  $a$  or total forcing  $at$ . Inserting numerical values ( $L = 2600\text{m}$ ,  $K = 350\text{Wm}^{-1}\text{K}^{-1}$ ,  $c = 4 \times 10^6\text{Jm}^{-3}\text{K}^{-1}$ ), we obtain  $\tau \approx 990$  years.

The approximation of the full solution with one decaying mode thus yields for the evolution of temperature and TOA energy imbalance:

$$T(t, z) \approx \frac{a}{\lambda}t - (1 - e^{-t/\tau})f(z) \quad (12)$$

$$N(t) \approx (1 - e^{-t/\tau})\frac{acL}{\lambda}. \quad (13)$$

With the slowest mode approximation, the decaying mode  $\tau = \tau_{sl}$  is the slowest decaying mode of the diffusive system and the term  $cL$  is the total heat capacity of the system  $C$ . The general form of the solutions 12-13 is valid for not only the diffusion equation. The one-layer model  $C \frac{dT_s}{dt} = F(t) - \lambda T_s(t)$  recovers the same solution but with a response timescale:  $\tau = C/\lambda$ . The two-box model (equations 2) also has the same solution form, with the repose timescale  $\tau$  depending on the two heat capacities, heat exchange coefficient and climate feedback parameter (see for example Appendix B.3 in Gregory et al. (2023)). The timescale provided by Watts et al. (1994) also depends on both  $C$  and  $\lambda$ . The disappearance of  $\lambda$  in the response timescale here is due to the approximation  $\lambda L \gg K$ . The timescale in a model with a diffusive domain is always longer than the timescale in the simplest one-layer model.

### 3. Physical intuition for the transient response: the growing apparent heat capacity

One can gain intuition for the transient response to monotonically increasing forcing by thinking of the system as a single layer with temperature  $T_s$  and a time-evolving heat capacity:

$$C_{\text{app}}(t) \frac{dT_s}{dt} = N = F - \lambda T_s \quad (14)$$

Here, the apparent heat capacity  $C_{\text{app}}$  is not a real physical heat capacity but arises as a mathematical concept describing the time-dependent influence of the diffusive domain. It can be diagnosed

as follows:  $C_{\text{app}} = \frac{N}{dT_s/dt} = \frac{Nd t}{dT_s} = \frac{E}{\Delta T_s}$ , where  $E$  is the accumulated energy in the system in Joules. The apparent heat capacity may be diagnosed from the instantaneous flux and temperature tendency,  $C_{\text{app}} = \frac{N}{dT_s/dt}$ , or from the integrated change in heat content  $E$  and the surface temperature change  $\Delta T_s$ ,  $C_{\text{app}} = \frac{\Delta E}{\Delta T_s}$ . Equivalently, we may define an apparent depth  $L_{\text{app}} = C_{\text{app}}/c$ , which is the apparent heat capacity expressed as equivalent ocean depth in meters.

Using the expressions for  $T(z=0)$  and  $N$  from equations 12 and 13, we can derive  $L_{\text{app}}(t)$  for the case of linearly increasing forcing:

$$L_{\text{app}} = \frac{\lambda(-1 + e^{t/\tau})L\tau}{-cL + \lambda\tau e^{t/\tau}} \xrightarrow{t \rightarrow \infty} L, \quad (15)$$

in which the dependence of the exact forcing rate  $a$  disappears. The increase of  $L_{\text{app}}$  over time indicates that close to the onset of the forcing growth, the system responds as a shallow reservoir and over time approaches the limit of the total domain depth  $L$ . This happens in tandem with the growing imbalance  $N$ . In QSS,  $L_{\text{app}} = L$  and  $N = \frac{acL}{\lambda}$ , and prior to QSS, both  $L_{\text{app}}$  and  $N$  increase logarithmically (see Figure 2 a, b).

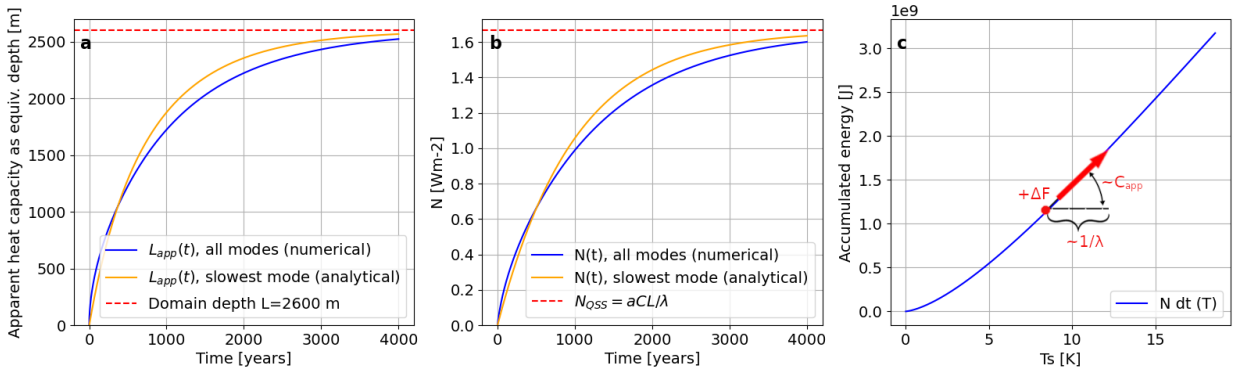


FIG. 2. Temporal evolution of the apparent heat capacity (a) and top of domain imbalance (b). Phase space of accumulated energy and surface temperature (c). Parameters are the same as in Figure 1.

One can describe the problem as partitioning a  $\Delta F$  over a short period of time ( $\Delta t \sim 1$  year) in an  $E(T)$  phase space (Figure 2 c). A part of the additional amount of forcing  $\Delta F$  will raise  $N$ , i.e. introduce a temperature tendency in the deeper layers and result in energy accumulation in the system, and the other part raises the surface temperature  $T_s$  and through the climate feedback decrease  $N$ . The angle in the  $E(T_s)$  phase space is  $C_{\text{app}}(t)$  and the projection on the  $T_s$ -axis is

proportional to  $1/\lambda$ . Before QSS,  $C_{\text{app}}(t)$  depends not only on  $L$  but also on  $K$  and  $\lambda$  (equation 15).

It is important to mention that  $C_{\text{app}}$  depends on the functional form of the forcing. For a Heaviside function ( $F(t \leq 0) = 0, F(t > 0) = \text{const}$  (e.g. the abrupt-4xCO<sub>2</sub> experiment),  $L_{\text{app}}$  will evolve initially from a very small value to a maximum that exceeds  $L$  as the deeper layers still experience a substantial temperature tendency, but the surface temperature is close to the steady state temperature. This limit is further discussed in Appendix C.

#### 4. Application for interpreting observations and models

##### *a. TCR when accounting for the forcing rate and response time scale*

We now use the analytical insights from the previous sections to interpret the temporal evolution of surface temperature and top of atmosphere imbalance in the 1pctCO<sub>2</sub> experiment. We wish to characterize the degree to which the system has approached QSS, which depends on the time at which the temperature tendency is evaluated ( $t'$ ) relative to the response time scale of the system ( $\tau$ ). A convenient metric is the ratio of the surface temperature tendency ( $\frac{dT(t)}{dt}$ ) relative to the corresponding steady state temperature tendency ( $\frac{dT_{\text{SS}}}{dt}$ ). The latter can be simply estimated using  $F_{2x}$  and  $\lambda$  from an abrupt-4xCO<sub>2</sub> run<sup>4</sup> as  $\frac{dT_{\text{SS}}}{dt} = \frac{a}{\lambda}$ . The equilibration time scale of the system is much longer than the 150-year length of 1pctCO<sub>2</sub> simulations. It is thus possible to approximate  $\frac{dT(t)}{dt}$  to the linear regression of the surface temperature over the entire 150-year period or any subset large enough to not be influenced by internal variability. It is not possible to obtain sufficient information to estimate the total heat capacity of the system from AOGCM simulations and we need to make an approximation for the total domain depth  $L$ : we set  $L = 2600\text{m}$  from the mean depth of the ocean 3682 m times its surface area fraction 71% as a first order estimate.

Figure 3 a shows the surface temperature under a 1pctCO<sub>2</sub> scenario – the liner regression will not capture the slight curvature in this evolution, but it is a good indicator for the state of the system as the curvature is due to faster decaying modes and our analytical approximation is only derived for the slowest one.

We use equation 12 to estimate the ratio of the derivatives analytically at any point  $t'$ :

---

<sup>4</sup>One can derive the forcing rate from  $F_{2x}$  as  $F(t) = F_{2x} \frac{\ln(1.01^t)}{\ln(2)}$ ,  $a = \frac{dF}{dt} = F_{2x} \frac{\ln(1.01)}{\ln(2)}$

$$\frac{dT(t=t')}{dt} / \frac{dT_{SS}}{dt} = 1 - \frac{K e^{-t'/\tau} \pi^2}{4\lambda L}, \quad (16)$$

which is the time-dependent correction one should apply to  $dT_{SS}/dt$  in order to estimate the transient tendency  $\frac{dT(t=t')}{dt}$  at time  $t'$ . This ratio will evolve from  $1 - \frac{K\pi^2}{4\lambda L} \approx 0.67$  to 1 from the onset of the forcing until the system approaches QSS<sup>5</sup>.

Going one step further, one can use equations 13 and 16 to obtain the expression:

$$\frac{dT/dt}{dT_{SS}/dt} = 1 - \frac{dN/dt}{dF/dt}, \quad (17)$$

which relates the rate of change of temperature to the rate of change of the TOA imbalance in the transient run. The ratios of these derivatives are obtained as linear regressions from models within the Copled Model Intercomparison – Phase 6 (CMIP6, Eyring et al. (2016)) and shown in the last two columns of Table 1. On average, the transient temperature evolves at 67% the rate of the SS temperature, and the ratio between the rates of change of  $N$  and  $F$  is therefore 33%. Over time,  $\frac{dT/dt}{dT_{SS}/dt}$  will increase at the expense of  $\frac{dN/dt}{dF/dt}$ .

If the ocean heat uptake efficacy ( $\epsilon$  in equation 2) is substantially different from 1, one needs to account for it in equation 17 as (see equation 14 in Winton et al. (2010)):

$$\frac{dT/dt}{dT_{SS}/dt} = 1 - \epsilon \frac{dN/dt}{dF/dt}, \quad (18)$$

Therefore, we can expect that models, for which the last two columns ( $\frac{dT}{dT_{SS}} + \frac{dN}{dF}$ ) in Table 1 do not sum to 1, to have  $\epsilon \neq 1$ .

### *b. Estimation of K from coupled models*

An equivalent approach to evaluating the time-dependent ratio  $\frac{dT(t)}{dt} / \frac{dT_{SS}}{dt}$  would be to solve equation 16 for  $K$ . We choose  $t'$  from the middle of the period over which we estimate the trend (we do this over the whole length of the 1pctCO2 run: 150 years, therefore  $t' = 75$ years). Knowing  $a$  and  $\lambda$  (we take the values estimated by Flynn and Mauritsen (2020)) and supposing that  $c = 4 \times 10^6 \text{ Jm}^{-3}\text{K}^{-1}$  and  $L = 2600\text{m}$ , we can solve equation 16 for  $K$ .  $K$  also appears in  $\tau$  and we solve the transcendental equation, but since  $\tau$  is very large, a similar solution would be obtained with  $t' = 0$ .

---

<sup>5</sup>We substitute  $t' = 0$  in equation 16,  $K = 350 \text{ Wm}^{-1}\text{K}^{-1}$ ,  $L = 2600 \text{ m}$ . The value of  $K$  is obtained from models.

TABLE 1. Heat equation parameters estimated from the 1pctCO2 and abrupt-4xCO2 runs by coupled models. The first 3 columns are copied from Flynn and Mauritsen (2020).  $K$  is estimated from eq. 16 and  $\gamma$  from eq. B6. The estimates of  $K$  and  $\gamma$  depend on the assumption for total domain depth  $L = 2600\text{m}$ . To estimate  $\gamma$ , we also suppose a ratio between the upper ( $C_1$ ) and deep layer ( $C_2$ ) heat capacities  $k = C_1/C_2 = 0.1$ .  $dT$  is the rate of temperature change,  $dT_{SS}$  is the rate of the corresponding temperature at flux equilibrium,  $dN$  is the rate of change of TOA imbalance,  $dF$  is the rate of forcing. The ratios of derivatives are based on linear regressions computed over the full length (150 years).

	TCR	$F_{2x}$	$\lambda$	$K$	$\gamma_{QSS}$	$dT/dT_{SS}$	$dN/dF$
	[K]	[ $\text{Wm}^{-2}\text{K}^{-1}$ ]	[ $\text{Wm}^{-2}\text{K}^{-1}$ ]	[ $\text{Wm}^{-1}\text{K}^{-1}$ ]	[ $\text{Wm}^{-2}\text{K}^{-1}$ ]		
				( $L=2600$ )	( $L=2600, k=0.1$ )		
BCC-ESM1	1.77	3.02	0.92	323	0.35	0.69	0.33
BCC-CSM2-MR	1.60	3.06	1.00	326	0.36	0.71	0.28
CESM2	1.99	3.19	0.62	332	0.36	0.53	0.42
CESM2-WACCM	1.92	3.26	0.62	365	0.40	0.48	0.43
CNRM-ESM2-1	1.82	2.96	0.62	304	0.33	0.56	0.45
CNRM-CM6-1	2.23	3.70	0.77	343	0.38	0.61	0.39
CNRM-ESM2-1	2.75	3.68	0.66	284	0.31	0.62	0.39
CNRM-CM6-1	2.91	3.28	0.62	189	0.21	0.72	0.30
EC-Earth3-Veg	2.76	3.34	0.80	240	0.26	0.73	0.26
GFDL-CM4	-	3.14	0.83	318	0.35	0.66	0.35
GFDL-ESM4	-	3.84	1.50	408	0.45	0.76	0.25
GISS-E2-1-G	1.66	3.84	1.48	-	-	-	-
GISS-E2-1-H	1.81	3.47	1.16	351	0.38	0.73	0.29
HadGEM3-GC31-LL	2.47	3.48	0.64	263	0.29	0.63	0.39
INM-CM4-8	1.30	2.64	1.46	204	0.22	0.87	0.13
IPSL-CM6A-LR	2.39	3.39	0.75	301	0.33	0.64	0.32
MIROC-ES2L	1.51	4.03	1.51	478	0.52	0.73	0.30
MIROC6	1.58	3.61	1.39	469	0.51	0.71	0.31
MPI-ESM1-2-HR	1.57	3.60	1.27	395	0.43	0.73	0.29
MRI-ESM2-0	-	3.37	1.08	491	0.54	0.61	0.36
NESM3	-	3.78	0.84	314	0.34	0.67	0.33
NorCPM1	1.55	3.58	1.29	425	0.46	0.71	0.31
NorESM2-LM	1.48	3.44	1.38	538	0.59	0.67	0.29
SAM0-UNICON	2.08	3.85	1.05	401	0.44	0.67	0.33
UKESM1-0-LL	2.79	3.56	0.67	286	0.31	0.62	0.38
Mean	1.98	3.44	1.00	348	0.38	0.67	0.33
5 <sup>th</sup> to 95 <sup>th</sup> p	[1.5, 2.8]	[3, 3.8]	[0.6, 1.5]	[210, 489]	[0.2, 0.5]	[0.5, 0.8]	[0.3, 0.4]

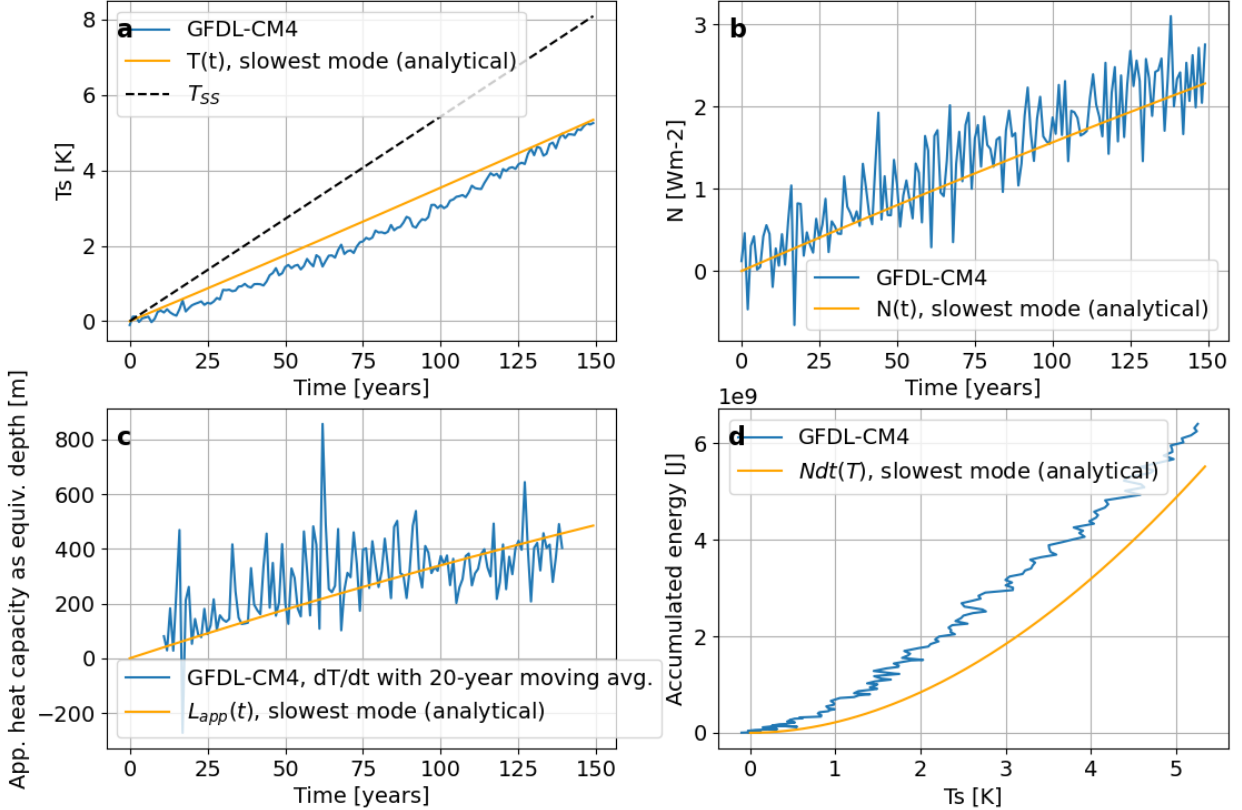


FIG. 3. Temporal evolution of surface temperature (a), top of atmosphere imbalance (b), effective heat capacity (c) and accumulated energy and surface temperature phase space (d). Blue lines correspond to the GFDL-CM4 1pctCO2 run (anomalies relative to piControl). Orange lines are the analytical approximation (equations 12-13) with  $F_{2x} = 3.13 \text{ Wm}^{-2}$ ,  $\lambda = 0.83 \text{ Wm}^{-2}\text{K}^{-1}$ ,  $K = 318 \text{ Wm}^{-1}\text{K}^{-1}$ ,  $L = 2600 \text{ m}$ .

The results for individual models are presented in Table 1 and the average value of  $K$  is around  $350 \text{ Wm}^{-1}\text{K}^{-1}$ .

If we return to the assumption of  $K$  being constant in depth, the values we provide for  $K$  are likely overestimates because in a 150-year period, the temperature evolution would be affected mainly by the mixing in the upper ocean layers.

We can relate our estimate of  $K$  to the exchange coefficient  $\gamma$  between the two layers in the two-box model (equation 2). This can be done because the two-box model QSS can be analytically derived from the QSS solution of the heat equation (equation 7) by defining  $T_1(t)$  and  $T_2(t)$  and as the integrals of  $T_{QSS}(t, z)$  over the appropriate depth intervals. The full derivation is provided in Appendix B. The estimated  $\gamma_{QSS}$  would be a consequence of the assumptions of domain depth

$(C_1 + C_2)$  and ratio of  $k = C_1/C_2$  and will evolve in time until QSS. We assume a domain depth of 2600 m and a ratio of 0.1. The average value of  $\gamma_{\text{QSS}}$  that we obtain in this way is around  $0.4 \text{ Wm}^{-2}\text{K}^{-1}$ .

Geoffroy et al. (2013b) have fitted the surface temperature evolution in the abrupt-4xCO<sub>2</sub> experiment to the 2-box model. The estimates of  $\gamma$  obtained by them within CMIP5 models are in the range  $0.5 - 1.1 \text{ Wm}^{-2}\text{K}^{-1}$ . Our estimate of  $\gamma_{\text{QSS}} = 0.4 \text{ Wm}^{-2}\text{K}^{-1}$  cannot be directly compared to the one from Geoffroy et al. (2013b) for two reasons: (1), we estimate  $\gamma_{\text{QSS}}$  which is the value  $\gamma$  would approach over time. Figure B1 indicates that when the heat equation is reduced to two boxes, initially  $\gamma$  is larger and decreases to  $\gamma_{\text{QSS}}$ ; (2), we do not have a good estimate for the true depth of the domain – we suppose  $L = 2600$  m based on the equivalent ocean depth. The domain depth estimated by Geoffroy et al. (2013b) is on the order of 700 m but this might be biased low due to the time-dependent effective heat capacity of the system and the finite length of the simulation - see Figure 3 c. Indeed, if we fit the first 150 years of the numerical solution of the diffusion model (equations 4, 5) with parameters  $\lambda = 1 \text{ Wm}^{-2}\text{K}^{-1}$ ,  $K = 350 \text{ Wm}^{-1}\text{K}^{-1}$ ,  $L = 2600$  m to the two-box model (equations 2), we obtain the parameter values  $\lambda = 1 \text{ Wm}^{-2}\text{K}^{-1}$ ,  $\epsilon \approx 1.3 \text{ Wm}^{-2}\text{K}^{-1}$ ,  $C_1 \approx 100\text{m}$ ,  $C_2 \approx 550\text{m}$ ,  $\gamma \approx 0.8 \text{ Wm}^{-2}\text{K}^{-1}$ , which are consistent with the values obtained in Geoffroy et al. (2013b,a).

This indicates that parameters of the two-box model estimated from a shorter period could overestimate  $\gamma$  and/or underestimate the domain depth and that these parameters should not be interpreted as general properties of the system. The parameters obtained by such a fit are still adequate in the temporal ranges over which the fit is performed and can be used to emulate climate of similar timescales. One should be careful if for example the parameters are estimated over a 10-year period and the two-box model is integrated for 100 years. Another culprit of diffusion models is that the system response depends on the initial state and it cannot be initialized with  $T_1 = T_2 = 0$  when the system is at disequilibrium  $T_1 \neq T_2$ .

### *c. Simple estimates of expected observational trends*

We test the analytical expressions from equations 12-13 against the observed trends in global mean surface temperature and top of atmosphere imbalance. Taking the time derivatives of  $T(t)$

and  $N(t)$ , one can estimate their tendencies under linearly increasing forcing  $F(t) = at$  as:

$$\frac{dT}{dt} = a - \frac{1 - e^{-t/\tau}}{\tau} \frac{aC}{\lambda} \quad (19)$$

$$\frac{dN}{dt} = \frac{e^{-t/\tau}}{\tau} \frac{aC}{\lambda} \quad (20)$$

Myhre et al. (2025) do point out that within climate models  $\frac{dN}{dt} \sim \frac{1}{\lambda}$ .

The historical forcing from greenhouse gasses can be approximated to a long period with weak linear forcing and a ramp up in the 1960s: from 1750 until 2025 (275 years) with a growth rate  $a_1 = 0.005 \text{ Wm}^{-2}\text{year}^{-1}$  and from 1965 to 2025 (60 years) with a growth rate  $a_2 = 0.04 \text{ Wm}^{-2}\text{year}^{-1}$  (Smith et al. 2021). Since the model is linear, the estimate at year 2025 can be obtained as a sum of the estimates for the two growth rates  $a_1$  and  $a_2$  at the year 2025.

Supposing realistic values of  $\lambda$ ,  $C$  and  $\tau$  can yield an order of magnitude estimate of the current state of the system and evaluate the structure of the diffusive model. Let  $\lambda = 1 \text{ Wm}^{-2}\text{K}^{-1}$ ,  $C = 10^{10} \text{ Jm}^2\text{K}^{-1}$ ,  $\tau = 1000$  years, then for the year 2025 one could expect a total temperature change of 2.6K, a temperature tendency of 0.3K/decade, a TOA imbalance of  $1.2 \text{ Wm}^{-2}$  and a trend in the TOA imbalance of  $0.1 \text{ Wm}^{-2}/\text{decade}$ . For comparison, the observed values which might be influenced by decadal-scale internal climate variability are  $T \approx 1.5\text{K}$ ,  $\frac{dT}{dt} \approx 0.3$  (based on the the ERA5 global reanalysis (Hersbach et al. 2020) but the trends vary across datasets (Menemenlis et al. 2025)), a TOA imbalance of  $N = 1.0 \pm 0.2 \text{ Wm}^{-2}$ ,  $dN/dt = 0.45 \pm 0.18 \text{ Wm}^{-2}/\text{decade}$  (Loeb et al. 2024).

To an order of magnitude, the estimates agree with observations and demonstrate the puzzling fact that the climate feedbacks have been stronger prior to the 1960s and have since weakened (e.g. Fueglistaler and Silvers (2021); Salvi et al. (2023)). The adjustment of the parameters in the energy balance framework discussed here cannot provide a better estimate of  $T$ ,  $N$  and their tendencies. Supposing that a bias in the observations or forcing estimates is unlikely and the influence of decadal-scale variability is not of such a magnitude, one is left to reshape the theoretical framework. Reshaping can include time-varying effective climate feedback (e.g. the efficacy factor in Winton et al. (2010); Held et al. (2010)), a more complex representation of vertical ocean mixing and/or a geometric structure which accounts not only for vertical but also meridional heat transport (as recently proposed by Gregory et al. (2023)).

## 5. Discussion and summary

Based on energy balance models which describe the atmosphere-ocean system using a surface feedback and vertical heat exchange below, we use the heat equation with energy-conservative boundary conditions to provide a simple analytical description of the transient climate response. The surface feedback  $\lambda$  is a property of the atmosphere and the heat conductivity in depth  $K$  represents the ocean mixing. The solution to this equation in response to linearly increasing forcing  $\frac{dF}{dt} = a$  can be approximated to:

$$T(t, z = 0) \approx \frac{a}{\lambda}t - (1 - e^{-t/\tau})\frac{acL}{\lambda^2}$$

$$N(t) \approx (1 - e^{-t/\tau})\frac{acL}{\lambda}$$

with a time scale  $\tau \approx \frac{c}{K} \frac{4L^2}{\pi^2}$ , which depends on the mixing coefficient  $K$  and the domain depth squared  $L^2$  and is on the order of thousands of years.

We relate this solution to the conventional definition of  $T_{TCR}$  as the temperature at the time of doubling of forcing in a 1pctCO2 scenario in AOGCM simulations. The response time scale  $\tau$  depends on  $K$  and  $L$  and it will vary between AOGCMs. In order to derive parameters that describe the intrinsic system properties from the conventional definition of  $T_{TCR}$ , one needs to account for the AOGCM-dependent timescale of response. The 150-year CMIP6 simulations are too short to estimate the total heat capacity of the system and we assume  $L = 2600\text{m}$  based on the effective ocean depth. This allows us to estimate the heat exchange coefficient  $K$  from the 1pctCO2 simulations given  $F_{2x}$  and  $\lambda$  (e.g  $F_{2x}$  and  $\lambda$  can be calculated from the abrupt-4xCO2 scenario). Since the response timescale is long, a linear regression of the surface temperature evolution over  $\sim 100$  years yields a good result. We suggest normalizing the linear trend (derivative) of the surface temperature evolution in a 1pctCO2 simulation to the derivative of the corresponding SS temperature  $\frac{dT_{SS}}{dt} = \frac{a}{\lambda}$ , which removes the dependence on the forcing rate  $a$ . In a short period immediately after the forcing onset, over which the evolution of the surface temperature is linear, this is equivalent to taking  $T_{TCR}/T_{ECS}$ . The resulting ratio is time-dependent and depends on  $K$  through the time scale of flux equilibration, and on  $\lambda$  and  $L$  through the offset between the steady state ( $T_{SS}$ ) and quasi-steady state temperatures ( $T_{QSS}$ ):

$$\frac{dT/dt}{dT_{SS}/dt} = \begin{cases} 1 - \frac{K\pi^2}{4\lambda L}, & t \rightarrow 0 \\ 1, & t/\tau \gg 1. \end{cases} \quad (21)$$

It evolves from around 0.67 near the forcing onset to 1 in quasi-steady state (equation 16 and Table 1). In other words, before reaching the quasi-steady state over thousands of years, the surface temperature would evolve further and further away from  $T_{SS}$  and the TOA imbalance will increase even for forcing with a linear growth.

The ocean mixing coefficient  $K$  can be estimated from  $\frac{dT(t)}{dt} / \frac{dT_{SS}}{dt}$  (equation 16), to be on the order of  $350 \text{ Wm}^{-1}\text{K}^{-1}$  in climate models. This would correspond to two-box model  $\gamma \approx 0.4 \text{ Wm}^{-2}\text{K}^{-1}$  or ocean diffusivity  $\kappa = \frac{K}{c} \approx 2 \times 10^5 \text{ m}^2\text{s}^{-1}$ . AOGCMs with a smaller  $K$  have a higher  $\frac{dT(t)}{dt} / \frac{dT_{SS}}{dt}$  and  $T_{TCR}$ . This estimate of  $K$  might be biased high because in a real ocean  $K = K(z)$  and a 150-year simulation allows us to only probe the first  $\sim 500$  m of the ocean.

The two-box model (Gregory 2000; Held et al. 2010) can be derived from the form of the heat equation discussed here – both are, in essence, a diffusion model forced at the top and with a surface temperature feedback. We note that the two apparent response timescales diagnosed from the surface temperature in abrupt-4xCO<sub>2</sub> experiments – an early rapid warming followed by a slower adjustment, needs not to be interpreted as two underlying heat-capacity reservoirs. Instead, this response arises from the inherent structure of a diffusive domain with a surface temperature feedback.

Such an energy balance framework gives a good order of magnitude estimate for the observed surface temperature and TOA imbalance tendencies. The framework is structurally limited because it does not include time-varying effective climate feedback (as is done by the inclusion of an efficacy factor in Held et al. (2010)) and the ocean heat transport is considered only vertically but not horizontally (as an expansion suggested in Gregory et al. (2023)).

*Acknowledgments.* I thank Stephan Fueglistaler for constructive input and feedback that shaped this paper. I am also grateful to Doris Folini for her continuous enthusiasm for math problems. The numerical solution of the heat equation was realized on the GPU machine set up and maintained by Daniel Tsvetkov and Denitsa Rusinova as a personal project.

The WCRP, CMIP6 modeling groups, and ESGF are acknowledged for enabling and providing the data.

The data analysis and visualization have been performed using free and open source software: a big thanks to the community for building powerful tools from which everyone can benefit.

B.C. is supported by Swiss National Science Foundation Grant P500PN\_222086.

*Data availability statement.* Wolfram Mathematica notebooks and analysis code are available at <https://gitlab.com/mjade/analytical-insights-into-tcr>. The version used in this study corresponds to commit 2a2f347c.

The CMIP6 archive can be accessed at <https://esgf-node.llnl.gov/projects/cmip6/>.

## APPENDIX A

### Derivation of slowest decaying mode

Equation 7 is the quasi-steady state solution of the heat equation (equation 4) with boundary conditions from equation 5, i.e. this is the long-term limit of the solution. We also want to obtain the full time-dependent solution to the heat equation, which describes the departure from the initial condition. For an unperturbed state in equilibrium (steady state), we set the initial condition to a constant profile in depth:

$$T(t = 0, z) = 0 \tag{A1}$$

In this case the full solution is given by:

$$T(t, z) = -\frac{a}{\lambda}t + \sum_{k_1=1}^{\infty} f(k_2(k_1))e^{-\frac{K}{C}k_2(k_1)t}, \tag{A2}$$

where the coefficients  $k_2$  are all possible roots of the transcendental equation:

$$\tan(L\sqrt{k_2}) = \frac{\lambda}{K\sqrt{k_2}} \tag{A3}$$

The first root of equation A3 is the largest and will give us the slowest decay mode  $e^{-\frac{t}{\tau_1}}$ , where the decay time is  $\tau_1 = \frac{c}{Kk_2(1)}$ . We can solve for  $k_2(1)$  by finding the first crossing point for the curves  $\tan(L\sqrt{x})$  and  $\frac{\lambda}{K\sqrt{x}}$ . Since all parameters are positive, we let  $u = \sqrt{x}/L$  and then the curves become  $f_1(u) = \tan(u)$  and  $f_2(u) = L\lambda/(Ku)$ . In the limit  $L\lambda \gg K$ , the first root approaches  $\pi/2$ . In the climate case, the climate feedback parameter  $\lambda$  is around  $1\text{Wm}^{-2}\text{K}^{-1}$ ; the depth of the ocean  $L$  is on the order of a few thousand of meters and the ocean turbulent diffusivity  $K$  is usually a few hundred  $\text{Wm}^{-1}\text{K}^{-1}$ . This gives us the slowest decaying mode:  $\tau_{sl} = \tau_1 \approx \frac{c}{K} \frac{4L^2}{\pi^2}$ .

If one further assumes that this is the only time-dependent mode which acts on the system to approach quasi-steady state, the approximation for the full solution can be written as equation 12:

$$T(t, z) \approx \frac{a}{\lambda} t - (1 - e^{-t/\tau_{sl}}) f(z),$$

where  $f(z) = \frac{-2acKL - 2a\lambda cLz + a\lambda cz^2}{2\lambda^2 K}$  is the quadratic depth profile that needs to be developed towards quasi-steady state.

This approximation can become invalid for the initial departure ( $t \rightarrow 0$ ) from the unperturbed profile in the deeper layers ( $z \rightarrow L$ ) for a large forcing rate  $a$ . If  $a$  is larger than the initial phase given by  $(1 - e^{-t/\tau_1})f(z)$ , then the temperature at levels where the QSS  $f(z)$  is small (i.e.  $z \rightarrow L$ ) might become negative. This solution is unrealistic and is due to the fact that we have neglected all other depth-dependent decaying time scales  $\tau_2, \tau_3, \dots$  that correspond to  $i = 2, 3, \dots$  in the full solution (equation A2).

This approximation can also underestimate  $\tau$  if  $K$  is sufficiently large, and the crossing point of  $f_1(u)$  and  $f_2(u)$  is before  $\frac{\pi}{2}$ .

Figure 1 shows both the full solution (evaluated numerically) and the approximation (evaluated analytically). The solution for the upper layers ( $z \rightarrow 0$ ) given by equation 12 is sufficiently accurate and the non-perfect match between the simulated temperature profile in depth (numerical solution) and its analytical solution at QSS (Figure 1 b) is due to a slight underestimation of  $\tau$  as mentioned above.

## APPENDIX B

### Analogy to the two-layer model

We use the QSS expression (equation 7) to derive an equivalent expression for the two-box model (equation 2), and we evaluate the two-box model's approach to QSS numerically.

We will use the full diffusion partial differential equation (equations 4, 5) to derive the two-box model of two coupled ordinary differential equations (equation 2). The temperatures of the two layers in the two-box model correspond to the vertically averaged temperatures in the full diffusion model, split at a certain depth ratio:

$$T_1 = \int_0^{kL} T(t, z) dz / (kL - 0) \quad (\text{B1})$$

$$T_2 = \int_{kL}^L T(t, z) dz / (L - kL) \quad (\text{B2})$$

The QSS solution to equations B1 and B2 is:

$$T_1 = \frac{a}{\lambda} t + \frac{acL(-6K + \lambda(-3 + k)kL)}{6\lambda^2 K} \quad (\text{B3})$$

$$T_2 = \frac{a}{\lambda} t + \frac{acL(-6K + \lambda(-2 + (-2 + k)k)L)}{6\lambda^2 K} \quad (\text{B4})$$

Obtaining  $T_1$  and  $T_2$  from the QSS solution  $T(t, z)$  in equation 7 allows us to backwards engineer  $\gamma$  from the original system (equation 2) as:

$$C_2 = (L - kL)c \quad (\text{B5})$$

$$\gamma_{\text{QSS}} = \frac{C_2 \frac{\partial T_2}{\partial z}}{T_1 - T_2} = K \frac{6(k-1)}{L(k-2)} \quad (\text{B6})$$

This equation links  $\gamma$  [ $\text{Wm}^{-2}\text{K}^{-1}$ ] to the heat conductivity  $K$  [ $\text{Wm}^{-1}\text{K}^{-1}$ ] and the coefficient  $k$  which splits the continuous finite domain of the heat equation solution to two finite layers. Based on the fits to climate models in (Geoffroy et al. 2013b), where  $L \approx 800$  m and the depth of the upper layer is  $\sim 80$  m, then  $k \approx 0.1$ .

The equation is time independent because it is based on the steady state solution, which allows us to obtain a clear expression. In the approach to steady state  $\gamma$  will evolve over time and approach the predicted value.

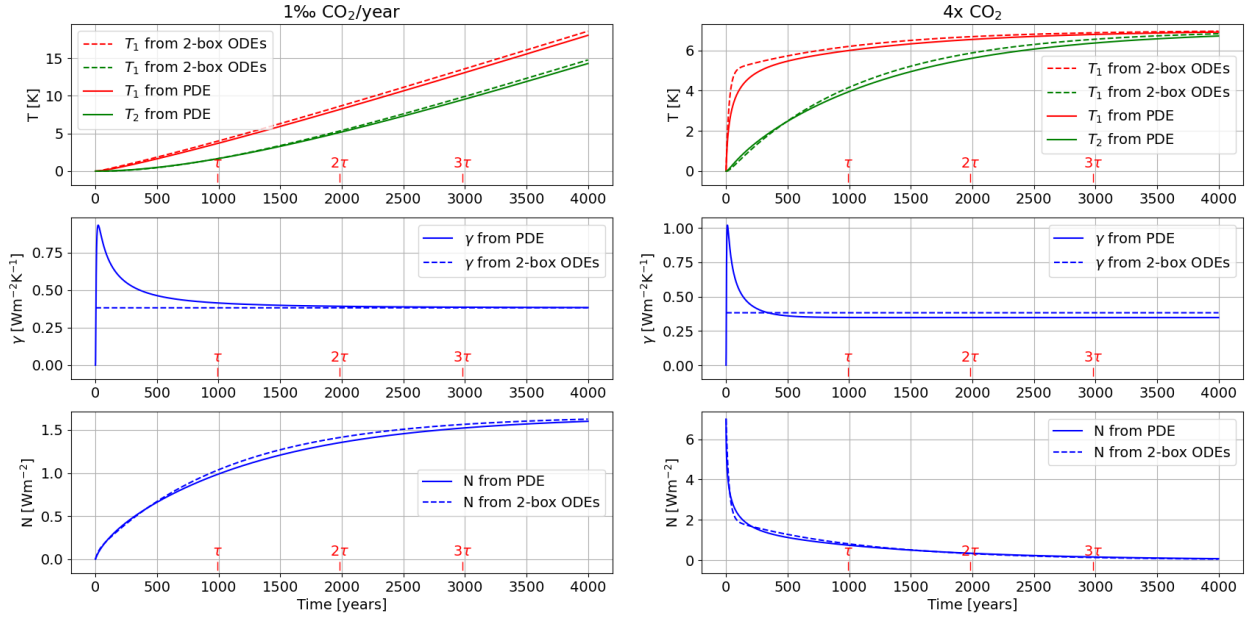


FIG. B1. Numerical solutions of the heat equation and the 2-layer model. Parameters for the heat equation are the same as in Figure 1; equivalent parameters for the 2-box model are chosen for  $k = 0.1$  and  $L = 2600$  m as  $C_1 = 260$  m,  $C_2 = 2340$  m, the equivalent  $\gamma$  is estimated to be  $0.38 \text{ Wm}^{-2}\text{K}^{-1}$ .

As seen in Figure B1 when the heat equation is reduced to the 2-box model,  $\gamma$  is larger in the beginning and approaches  $\gamma_{\text{QSS}}$  from equation B6, which we estimate analytically. Since  $\gamma$  is usually estimated from coupled models, i.e. done the other way around, it is likely that the fitted parameter is biased high if one wants to compare it to the heat equation.

We briefly note that the heat capacities have different units: in equation 4 we use the volumetric heat capacity  $c$  [ $\text{Jm}^{-3}\text{K}^{-1}$ ], while in the two-box model (equation 2) the heat capacities relate the temperature tendencies directly to energy fluxes, and hence have the units  $C_1, C_2$  [ $\text{Jm}^{-2}\text{K}^{-1}$ ], which is sometimes expressed as  $C_1, C_2$  [ $\text{W year}^{-1} \text{ m}^{-2} \text{ K}^{-1}$ ] (Geoffroy et al. 2013b).

## APPENDIX C

### The apparent heat capacity for $F = at$ and $F = const$

The temporal evolution and upper limit of the apparent heat capacity depends on the functional form of the forcing. We derive the lower and upper limits for the case of linearly increasing forcing  $F = at$  (e.g. 1pctCO2) and the Heaviside case of abrupt constant forcing  $F = const$  (e.g. abrupt-4xCO2).

Starting from the two-box model as in equation 2, one can diagnose the apparent heat capacity from the total temperature tendency of the system:

$$N = C_1 \frac{dT_1}{dt} + C_2 \frac{dT_2}{dt} \quad (C1)$$

$$C_{app} = \frac{N}{dT_1/dt} = C_1 + C_2 \frac{dT_2}{dT_1} \quad (C2)$$

And normalize to the volumetric heat capacity of sea water  $c = 4 \times 10^6$  [Jm<sup>-3</sup>K<sup>-1</sup>] to get the apparent ocean depth  $L_{app} = C_{app}/c$  in meters.

For  $F = at$  the upper limit of  $C_{app}$  is QSS, where  $\frac{dT_1}{dt} = \frac{dT_2}{dt} = \frac{a}{\lambda}$ , therefore  $C_{app} = C_1 + C_2$ , which is the domain depth or total heat capacity of the system.

For  $F = const$ , which is a Heaviside relaxation case, as time evolves the temperature tendency in the deeper layer  $\frac{dT_2}{dt}$  becomes larger than the one of the upper layer  $\frac{dT_1}{dt}$  and they both decrease with time as the system approaches flux equilibrium. An interesting feature is that the ratio of the temperature tendencies is constant and therefore  $C_{app}$  has an upper limit that is reached at some point in time before flux equilibrium. The upper limit of the ratio of the temperature tendencies is:

$$\frac{dT_2}{dT_1} = \frac{-\gamma C_1 + \sqrt{(\gamma C_1 + C_2(\gamma\epsilon + \lambda))^2 - 4\gamma C_1 C_2 \lambda} + \gamma C_2 \epsilon + C_2 \lambda}{2\gamma C_2 \epsilon}, \quad (C3)$$

which for  $C_1 \rightarrow 0$  evaluates to  $\lim_{C_1 \rightarrow 0} \frac{dT_2}{dT_1} = \frac{\lambda + \epsilon\gamma}{\epsilon\gamma}$ .

Since  $\frac{dT_2}{dt} > \frac{dT_1}{dt}$ , the upper limit of the apparent heat capacity for the  $F = const$  forcing form will be higher than the total system heat capacity.

The temporal evolution of  $C_{app}$  for the full-diffusion PDE and 2-layer model with both forms of forcing is shown in Figure C1.

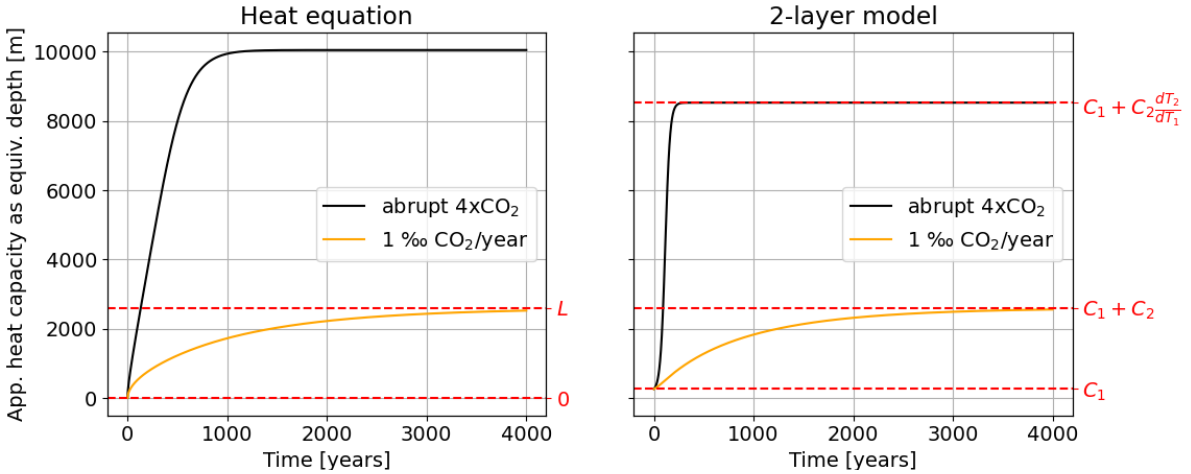


FIG. C1. The apparent heat capacity as equivalent depth for different functional forms of the forcing diagnosed from the numerical solution of the heat equation (left) and diagnosed from the two-layer model (right). Model parameters are the same as in Figure B1.  $dT_2/dT_1$  is calculated from equation C3 with  $\epsilon = 1$ .

The lower limit of  $C_{app}$  is 0 for the full-diffusion model (heat equation) and  $C_1$  for the two-layer model.

An important take-home message is that the two apparent response timescales often inferred from the surface temperature abrupt-4xCO<sub>2</sub> experiments – the rapid initial rise followed by a more gradual extended warming (see right panel on Figure B1), do not necessarily reflect the presence of two distinct heat-capacity reservoirs (such as  $C_1$  and  $C_2$ ). Instead, these features emerge from the structure of a diffusive domain with a surface temperature feedback. In such systems, the continuum of diffusive modes projects onto the surface temperature in a way that appears as a fast and a slow component, even though only a single physical heat capacity is specified.

## References

- Alexandrov, A. A., K. A. Orlov, and M. V. Butakova, 2017: Releases from the international association for the properties of water and steam for calculating properties of steam, ordinary and heavy water substance and seawater. *Journal of Physics: Conference Series*, **891**, 012 329, <https://doi.org/10.1088/1742-6596/891/1/012329>.
- Eyring, V., S. Bony, G. A. Meehl, C. A. Senior, B. Stevens, R. J. Stouffer, and K. E. Taylor, 2016: Overview of the coupled model intercomparison project phase 6 (cmip6) experimental

- design and organization. *Geoscientific Model Development*, **9** (5), 1937–1958, <https://doi.org/10.5194/gmd-9-1937-2016>.
- Flynn, C. M., and T. Mauritsen, 2020: On the climate sensitivity and historical warming evolution in recent coupled model ensembles. *Atmospheric Chemistry and Physics*, **20** (13), 7829–7842, <https://doi.org/10.5194/acp-20-7829-2020>.
- Frölicher, T. L., J. L. Sarmiento, D. J. Paynter, J. P. Dunne, J. P. Krasting, and M. Winton, 2015: Dominance of the southern ocean in anthropogenic carbon and heat uptake in cmip5 models. *Journal of Climate*, **28** (2), 862–886, <https://doi.org/10.1175/jcli-d-14-00117.1>.
- Fueglistaler, S., and L. Silvers, 2021: The peculiar trajectory of global warming. *Journal of Geophysical Research: Atmospheres*, **126** (4), <https://doi.org/10.1029/2020jd033629>.
- Gent, P. R., and J. C. McWilliams, 1990: Isopycnal mixing in ocean circulation models. *Journal of Physical Oceanography*, **20** (1), 150 – 155, [https://doi.org/10.1175/1520-0485\(1990\)020<0150:IMIOCM>2.0.CO;2](https://doi.org/10.1175/1520-0485(1990)020<0150:IMIOCM>2.0.CO;2).
- Geoffroy, O., D. Saint-Martin, G. Bellon, A. Voldoire, D. J. L. Olivié, and S. Tytéca, 2013a: Transient climate response in a two-layer energy-balance model. part ii: Representation of the efficacy of deep-ocean heat uptake and validation for cmip5 aogcms. *Journal of Climate*, **26** (6), 1859–1876, <https://doi.org/10.1175/jcli-d-12-00196.1>.
- Geoffroy, O., D. Saint-Martin, D. J. L. Olivié, A. Voldoire, G. Bellon, and S. Tytéca, 2013b: Transient climate response in a two-layer energy-balance model. part i: Analytical solution and parameter calibration using cmip5 aogcm experiments. *Journal of Climate*, **26** (6), 1841–1857, <https://doi.org/10.1175/jcli-d-12-00195.1>.
- Gnanadesikan, A., 1999: A simple predictive model for the structure of the oceanic pycnocline. *Science*, **283** (5410), 2077–2079, <https://doi.org/10.1126/science.283.5410.2077>.
- Gregory, J. M., 2000: Vertical heat transports in the ocean and their effect on time-dependent climate change. *Climate Dynamics*, **16** (7), 501–515, <https://doi.org/10.1007/s003820000059>.
- Gregory, J. M., T. Andrews, and P. Good, 2015: The inconstancy of the transient climate response parameter under increasing co<sub>2</sub>. *Philosophical Transactions of the Royal Society A:*

*Mathematical, Physical and Engineering Sciences*, **373 (2054)**, 20140417, <https://doi.org/10.1098/rsta.2014.0417>.

Gregory, J. M., and P. M. Forster, 2008: Transient climate response estimated from radiative forcing and observed temperature change. *Journal of Geophysical Research: Atmospheres*, **113 (D23)**, <https://doi.org/10.1029/2008jd010405>.

Gregory, J. M., and Coauthors, 2023: A new conceptual model of global ocean heat uptake. *Climate Dynamics*, **62 (3)**, 1669–1713, <https://doi.org/10.1007/s00382-023-06989-z>.

Held, I. M., M. Winton, K. Takahashi, T. Delworth, F. Zeng, and G. K. Vallis, 2010: Probing the fast and slow components of global warming by returning abruptly to preindustrial forcing. *Journal of Climate*, **23 (9)**, 2418–2427, <https://doi.org/10.1175/2009jcli3466.1>.

Hersbach, H., and Coauthors, 2020: The era5 global reanalysis. *Quarterly Journal of the Royal Meteorological Society*, **146 (730)**, 1999–2049, <https://doi.org/10.1002/qj.3803>.

Hoffert, M. I., A. J. Callegari, and C. Hsieh, 1980: The role of deep sea heat storage in the secular response to climatic forcing. *Journal of Geophysical Research: Oceans*, **85 (C11)**, 6667–6679, <https://doi.org/10.1029/jc085ic11p06667>.

IPCC, 2023: *Climate Change 2021 – The Physical Science Basis: Working Group I Contribution to the Sixth Assessment Report of the Intergovernmental Panel on Climate Change*. Cambridge University Press, <https://doi.org/10.1017/9781009157896>, URL <http://dx.doi.org/10.1017/9781009157896>.

Jeevanjee, N., D. J. Paynter, J. P. Dunne, L. T. Sentman, and J. P. Krasting, 2025: A holistic view of climate sensitivity. *Annual Review of Earth and Planetary Sciences*, **53 (1)**, 367–396, <https://doi.org/10.1146/annurev-earth-040523-014302>.

Kostov, Y., K. C. Armour, and J. Marshall, 2014: Impact of the atlantic meridional overturning circulation on ocean heat storage and transient climate change. *Geophysical Research Letters*, **41 (6)**, 2108–2116, <https://doi.org/10.1002/2013gl058998>.

Kuhlbrodt, T., and J. M. Gregory, 2012: Ocean heat uptake and its consequences for the magnitude of sea level rise and climate change. *Geophysical Research Letters*, **39 (18)**, <https://doi.org/10.1029/2012gl052952>.

- Lebedeff, S. A., 1988: Analytic solution of the box diffusion model for a global ocean. *Journal of Geophysical Research: Atmospheres*, **93 (D11)**, 14 243–14 255, <https://doi.org/10.1029/jd093id11p14243>.
- Liu, M., B. J. Soden, G. A. Vecchi, and C. Wang, 2023: The spread of ocean heat uptake efficiency traced to ocean salinity. *Geophysical Research Letters*, **50 (4)**, <https://doi.org/10.1029/2022gl100171>.
- Loeb, N. G., S.-H. Ham, R. P. Allan, T. J. Thorsen, B. Meyssignac, S. Kato, G. C. Johnson, and J. M. Lyman, 2024: Observational assessment of changes in earth's energy imbalance since 2000. *Surveys in Geophysics*, **45 (6)**, 1757–1783, <https://doi.org/10.1007/s10712-024-09838-8>.
- Loeb, N. G., G. C. Johnson, T. J. Thorsen, J. M. Lyman, F. G. Rose, and S. Kato, 2021: Satellite and ocean data reveal marked increase in earth's heating rate. *Geophysical Research Letters*, **48 (13)**, <https://doi.org/10.1029/2021gl093047>.
- Meehl, G. A., C. A. Senior, V. Eyring, G. Flato, J.-F. Lamarque, R. J. Stouffer, K. E. Taylor, and M. Schlund, 2020: Context for interpreting equilibrium climate sensitivity and transient climate response from the cmip6 earth system models. *Science Advances*, **6 (26)**, <https://doi.org/10.1126/sciadv.aba1981>.
- Menemenlis, S., G. A. Vecchi, W. Yang, S. Fueglistaler, and S. P. Raghuraman, 2025: Consequential differences in satellite-era sea surface temperature trends across datasets. *Nature Climate Change*, **15 (8)**, 897–903, <https://doi.org/10.1038/s41558-025-02362-6>.
- Morantine, M. C., and R. G. Watts, 1994: Time scales in energy balance climate models: 2. the intermediate time solutions. *Journal of Geophysical Research: Atmospheres*, **99 (D2)**, 3643–3653, <https://doi.org/10.1029/93jd01866>.
- Munk, W., and C. Wunsch, 1998: Abyssal recipes ii: energetics of tidal and wind mixing. *Deep Sea Research Part I: Oceanographic Research Papers*, **45 (12)**, 1977–2010, [https://doi.org/10.1016/s0967-0637\(98\)00070-3](https://doi.org/10.1016/s0967-0637(98)00070-3).
- Munk, W. H., 1966: Abyssal recipes. *Deep Sea Research and Oceanographic Abstracts*, **13 (4)**, 707–730, [https://doi.org/10.1016/0011-7471\(66\)90602-4](https://doi.org/10.1016/0011-7471(66)90602-4).

- Myhre, G., O. Hodnebrog, N. Loeb, and P. M. Forster, 2025: Observed trend in earth energy imbalance may provide a constraint for low climate sensitivity models. *Science*, **388** (6752), 1210–1213, <https://doi.org/10.1126/science.adt0647>.
- Newsom, E., L. Zanna, and J. Gregory, 2023: Background pycnocline depth constrains future ocean heat uptake efficiency. *Geophysical Research Letters*, **50** (22), <https://doi.org/10.1029/2023gl1105673>.
- Nijssen, F. J. M. M., P. M. Cox, and M. S. Williamson, 2020: Emergent constraints on transient climate response (tcr) and equilibrium climate sensitivity (ecs) from historical warming in cmip5 and cmip6 models. *Earth System Dynamics*, **11** (3), 737–750, <https://doi.org/10.5194/esd-11-737-2020>.
- Nikurashin, M., and G. Vallis, 2011: A theory of deep stratification and overturning circulation in the ocean. *Journal of Physical Oceanography*, **41** (3), 485–502, <https://doi.org/10.1175/2010jpo4529.1>.
- Raper, S. C. B., J. M. Gregory, and R. J. Stouffer, 2002: The role of climate sensitivity and ocean heat uptake on aogcm transient temperature response. *Journal of Climate*, **15** (1), 124 – 130, [https://doi.org/10.1175/1520-0442\(2002\)015<0124:TROCSA>2.0.CO;2](https://doi.org/10.1175/1520-0442(2002)015<0124:TROCSA>2.0.CO;2).
- Redi, M. H., 1982: Oceanic isopycnal mixing by coordinate rotation. *Journal of Physical Oceanography*, **12** (10), 1154 – 1158, [https://doi.org/10.1175/1520-0485\(1982\)012<1154:OIMBCR>2.0.CO;2](https://doi.org/10.1175/1520-0485(1982)012<1154:OIMBCR>2.0.CO;2).
- Rogers, M., R. Ferrari, and L.-P. Nadeau, 2023: Middepth recipes. *Journal of Physical Oceanography*, **53** (7), 1753–1766, <https://doi.org/10.1175/jpo-d-22-0225.1>.
- Rose, B. E. J., and L. Rayborn, 2016: The effects of ocean heat uptake on transient climate sensitivity. *Current Climate Change Reports*, **2** (4), 190–201, <https://doi.org/10.1007/s40641-016-0048-4>.
- Salvi, P., J. M. Gregory, and P. Ceppi, 2023: Time-evolving radiative feedbacks in the historical period. *Journal of Geophysical Research: Atmospheres*, **128** (20), <https://doi.org/10.1029/2023jd038984>.

- Smith, C., and Coauthors, 2021: Ipcw working group 1 (wg1) sixth assessment report (ar6) annex iii extended data. Zenodo, URL <https://zenodo.org/record/5705391>, <https://doi.org/10.5281/ZENODO.5705391>.
- Watts, R. G., M. C. Morantine, and K. Achuta Rao, 1994: Timescales in energy balance climate models: 1. the limiting case solutions. *Journal of Geophysical Research: Atmospheres*, **99 (D2)**, 3631–3641, <https://doi.org/10.1029/93jd01867>.
- Wigley, T. M. L., and M. E. Schlesinger, 1985: Analytical solution for the effect of increasing co2 on global mean temperature. *Nature*, **315 (6021)**, 649–652, <https://doi.org/10.1038/315649a0>.
- Winton, M., K. Takahashi, and I. M. Held, 2010: Importance of ocean heat uptake efficacy to transient climate change. *Journal of Climate*, **23 (9)**, 2333–2344, <https://doi.org/10.1175/2009jcli3139.1>.